Available online at www.sciencedirect.com
ScienceDirect
Journal of Power Sources 171 (2007) 477–482
JOURNAL OF POWER SOURCES
www.elsevier.com/locate/jpowsour

Short communication

Performance of metal-supported SOFCs with infiltrated electrodes

Michael C. Tucker*, Grace Y. Lau, Craig P. Jacobson, Lutgard C. DeJonghe, Steven J. Visco

Lawrence Berkeley National Laboratory, Materials Science Division, 1 Cyclotron Rd., MS 62-203, Berkeley, CA 94720, United States

Received 9 May 2007; received in revised form 13 June 2007; accepted 15 June 2007
Available online 23 June 2007

Abstract

Metal-supported solid oxide fuel cells (SOFCs) with thin YSZ electrolyte films and infiltrated Ni and LSM catalysts are operated in the temperature range 650–750 °C. A five-layer structure consisting of porous metal-support/porous YSZ interlayer/dense YSZ electrolyte film/porous YSZ interlayer/porous metal current collector is prepared at 1300 °C in reducing atmosphere. This cell structure is then sealed and joined to a cell housing/gas manifold using a commercially available braze. Finally, the porous YSZ interlayers are infiltrated with Ni and LSM catalyst precursor solutions at low temperature prior to cell testing. Infiltrating the catalysts after the high temperature sintering and brazing steps avoids undesirable decomposition of LSM, Ni coarsening, and interdiffusion between Ni catalyst and FeCr in the support. Maximum power densities of 233 and 332 mW cm^{-2} were achieved at 650 and 700 °C, respectively, with air as oxidant. With pure oxygen as oxidant, power densities of 726, 993, and >1300 mW cm^{-2} were achieved at 0.7 V at 650, 700, and 750 °C, respectively.
Published by Elsevier B.V.

Keywords: Solid oxide fuel cell; Metal-support; Infiltration

1. Introduction

Solid oxide fuel cell (SOFC) technology has achieved a very high level of technical refinement over more than 50 years of development. Large stationary power plants incorporating SOFC stacks have been demonstrated throughout the world, with impressive technical results. The cost of today's state-of-the-art SOFC technology remains, however, much too high to compete with entrenched power generation technologies. Forthcoming metal-supported SOFCs are expected to be competitive in the power generation equipment market because of the strength, tolerance to extremely rapid thermal cycling, and reduced materials cost that the metal-support provides.

Inexpensive FeCr-based ferritic stainless steels are the preferred metallic support material due to their low cost, adequate coefficient of thermal expansion (CTE) match with YSZ, and low oxidation rates suitable for the long lifetimes desired for SOFC power plants [1–6]. Balancing the competing requirements of longevity and performance leads us to expect an optimum operating temperature of 650–700 °C. Setting the SOFC temperature in this range also allows the balance of plant (BOP), manifolds, cell-to-cell joints, etc. to be made of inexpensive stainless steels as well. This minimizes cost for the entire system, not just the SOFC stack itself. Of course, metal-supported SOFCs can be operated above 700 °C for short periods of time, but increasing the operating temperature even to 800 °C would severely limit lifetime due to accelerated oxide scale growth.

Introducing ferritic stainless steel to the materials set introduces a number of challenges that must be overcome before successful deployment of metal-supported SOFC technology. These challenges include Cr poisoning, achieving high performance at low operating temperature, and difficulties with co-processing the metal-support and electrocatalysts. Poisoning of the cathode by Cr evolved from the steel surface has been a long-standing concern. Much progress has been made in the use of coatings to alleviate this problem. For instance, Topsoe Fuel Cells has demonstrated a stack operating with coated FeCr-based interconnects that generated power for 13,000 h with minimal degradation [7]. We address the challenges of performance and co-processing by infiltrating catalyst particles after cell fabrication, as discussed below.

Whereas traditional all-ceramic SOFCs can be cosintered at 1200–1400 °C in air, cosintering with metal support requires reducing atmosphere in order to avoid oxidation of the metal. Cathode catalysts such as LSM and LSCF decompose in reduc-

* Corresponding author. Tel.: +1 510 486 5304; fax: +1 510 486 4881.
E-mail address: mctucker@ibl.gov (M.C. Tucker).

0378-7753/$ – see front matter. Published by Elsevier B.V.
doi:10.1016/j.jpowsour.2007.06.076

ing atmosphere at elevated temperature, precluding them from being cofired with the anode and support structure [2,8]. A similar issue is encountered when braze-sealing SOFCS. Metal supported SOFC technology enables the use of brazed seals and joints that can withstand extremely rapid thermal cycling [9]. This offers the promise of rapid SOFC startup, and tolerance to large thermal gradients. Brazing requires a vacuum or inert atmosphere, however, and is therefore incompatible with cathode catalysts as well. For these reasons, a single-step infiltration process has been developed that allows the cathode catalyst to be introduced to the cathode structure after the cosintering and brazing steps [10,11]. In that work, infiltrated LSM was shown to support high current density and provided stable operation for over 500 h.

Our early metal-supported SOFC development efforts were based on a cofired metal support/Ni-YSZ anode/YSZ electrolyte trilayer structure, to which a cathode was added as an additional processing step, as depicted in Fig. 1a [2,3]. Maximum power density of about 100 mW cm^{-2} at 800 °C was achieved at that time. Cofiring a Ni-based anode at high temperature in reducing atmosphere, however, leads to coarsening of the Ni particles to unacceptably large particle size, as discussed below. Furthermore, if the anode layer directly contacts the metallic-support, significant Ni, Fe, and Cr interdiffusion between the Ni catalyst and support is a concern. This can lead to poor performance of the catalyst and changes in the CTE, mechanical properties or oxidation resistance of the support [12]. Inserting a diffusion barrier layer between the anode and support layers addresses this problem, but does not address the issue of coarsening. A metal-supported SOFC utilizing a barrier layer and plasma-sprayed YSZ electrolyte was recently reported [13]. The cell achieved a power density of 400 mW cm^{-2} at 800 °C, and was operated for 2300 h providing confidence in the potential stability of metal-supported SOFCs with YSZ electrolyte. We address the issues of Ni coarsening and interdiffusion by infiltrating the anode catalyst after all high-temperature processing operations are complete, as outlined in Fig. 1b. The infiltration process set forth by Sholklapper et al. [10,11] is modified in this work to provide infiltration of a well-connected, nanoparticulate Ni network into porous YSZ to form a complete SOFC anode with considerable triple-phase boundary. A similar approach has been taken previously to prepare Cu/CeO_2 dispersed on a porous YSZ framework [14]. Here, a metal-supported SOFC structure consisting of porous metal support, porous YSZ interlayer, dense YSZ electrolyte, porous YSZ interlayer, and porous metal current collector is fabricated at high temperature in reducing atmosphere. This is followed by braze-sealing the cell, and finally by infiltration of the anode and cathode catalysts at low temperature before fuel cell operation.

In this work, metal-supported SOFCs with thin YSZ electrolyte films and infiltrated Ni and LSM catalysts are produced. Very high current density is achieved at operating temperatures in the range 650–750 °C. We believe the power densities reported in this work are unsurpassed by any other metal-supported YSZ-electrolyte SOFC technology. The progress reported here substantially reduces the technical risk associated with metal-supported SOFCs; we anticipate widespread commercialization of this technology in the future.

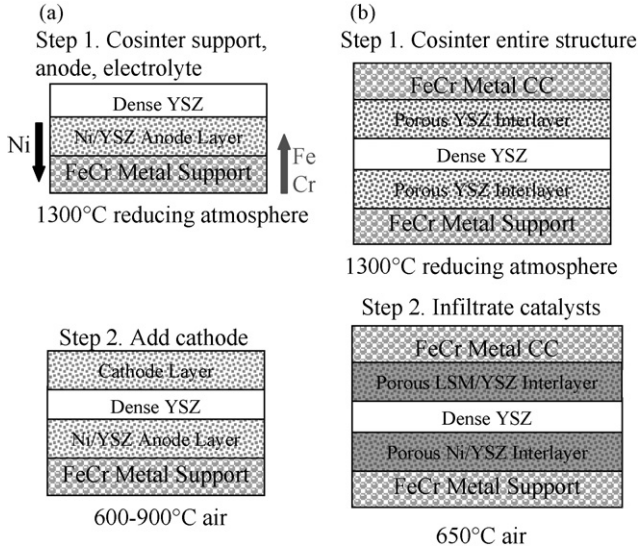

Fig. 1. Metal-supported SOFC preparation schemes. (a) Cosintering with Ni catalyst present, followed by application of cathode layer. Arrows indicate interdiffusion between anode and support layers. (b) Cosintering with catalysts absent, followed by catalyst infiltration.

2. Experimental methods

2.1. Cell fabrication

Tubular metal-supports were produced by isostatically pressing (10 kpsi, 5 min) a mixture of commercially available ferritic stainless steel powder (Ametek) and polymer binder/poreformer as described previously [15]. A porous YSZ interlayer was then applied to one side of the metal-support via a proprietary technique, followed by aerosol spray deposition of the thin YSZ electrolyte layer from an isopropanol-based solution, as described elsewhere [2]. This three-layered structure was sintered in reducing atmosphere (4% H_2/96% Ar) tube furnace at 1300 °C for 4 h, achieving a final diameter of roughly 1 cm. After inspecting the electrolyte for uniformity and full density, another interlayer of porous YSZ was applied to the electrolyte by a colloidal deposition technique, followed by a porous stainless steel current collector layer. The area of these layers determined cell active area, in the range 1.7–2.5 cm^2 for the cells tested here. The resulting five-layer structure was cofired in 4% H_2/96% Ar at 1250–1300 °C for 4 h. All YSZ powders were provided by Tosoh Corp. Several cells were produced with a mixture of NiO (green, J.T. Baker) and YSZ replacing the middle porous YSZ layer of the three-layer structure. All other processing was identical to the YSZ-only cells, except that the sintered Ni/YSZ layer was not infiltrated with more Ni before testing.

2.2. Braze sealing

After sintering, vacuum brazing was used to seal and join the cells to housings/gas manifolds machined from dense ferritic stainless steel. A 10:1 by weight mixture of Ticusil (Morgan

Advanced Ceramics) braze powder and TiH_2 powder (Alfa Aesar) was applied to the joint/seal area, followed by vacuum brazing. Brazing was carried out in an atmosphere of $<10^{-5}$ Torr at 910 °C for 10 min, with 15 °C min^{-1} heating and cooling rates. Quality of the braze seal was assessed by pressurizing the manifolded cell to 10 psi air pressure and checking for bubbles after submerging the cell in an acetone bath.

2.3. Catalyst infiltration

Catalyst infiltration essentially followed the procedure set forth in ref. [10]. Precursor solutions of nitrate salts (Sigma–Aldrich) were mixed with Triton-X-100 or Triton-X-45 (Union Carbide Chemicals and Plastics Co., Inc.) at surfactant loading of 0.3 g per 2 g of resulting catalyst particles. The salts were mixed in stoichiometric ratios to obtain "LSM" ($La_{0.85}Sr_{0.15}MnO_3$) or "Ni" (Ni–0.1CeO_2). The nitrate salt/surfactant mixtures were melted in an oil bath held at ~100 °C. Cells were heated to 100 °C in a box furnace, catalyst precursor solutions were applied to porous metal/YSZ layers of the cells, and the pores of the porous metal/YSZ layers were flooded by applying and releasing vacuum (200 mbar) twice in a vacuum impregnation apparatus (Epovac, Struers). Excess precursor solution was then removed from the cells, after which they were fired in air to 650 °C for 15 min to convert the nitrate salts to metal oxides. This process was repeated to build up catalyst concentration within the pores of the porous metal/YSZ structure. Both the porous YSZ layers and the metal-support and current collectors were coated with catalyst by this process.

2.4. Cell operation and testing

After catalyst infiltration, cells were mounted with Swagelok fittings to a test rig that provided flow of oxidant (dry air or pure oxygen) and moist hydrogen (3% H_2O) to the LSM-containing and Ni-containing sides of the cell, respectively. Pt wire electrical leads were spot welded directly to the metallic current collector and stainless steel cell housing, which was electrically connected to the metal cell support by braze. After flushing the test rig with oxidant and fuel streams, cells were heated to operating temperatures in the range 650–750 °C at a heating rate of 25 °C min^{-1}. Polarization curves were obtained using LabView software controlling a power supply (Kepco). AC impedance spectra were obtained with a potentiostat/frequency response analyzer (Solartron 1286/1255) in frequency sweep mode from 10^6 to 0.1 Hz.

2.5. SEM analysis

SEM images were obtained with a Hitachi S-4300SE/N scanning electron microscope in secondary electron imaging mode.

3. Results and discussion

Trilayer structures consisting of metal-support/Ni-YSZ anode/YSZ electrolyte were prepared at 1300 °C in reducing atmosphere. One such structure was cross-sectioned and polished before imaging. Fig. 2 shows the Ni-YSZ anode after sintering. The <3 μm NiO particles are reduced to Ni during sintering, allowing substantial coarsening and agglomeration as seen in the figure. Such coarsening reduces the amount of triple-phase boundary, and limits electrical connectivity throughout the Ni network. We presume Ni and FeCr interdiffusion occurred as well, although this was not analyzed. An LSCF cathode with Pt current collector was applied to such a cell, and the performance of the resulting SOFC was assessed at 700–800 °C. The impedance of the cell, shown in Fig. 3 to be over 15 Ω cm^2 at 800 °C, was unacceptably high. The high ohmic and electrode arc impedances are consistent with poorly connected Ni particles and low triple-phase boundary, respectively.

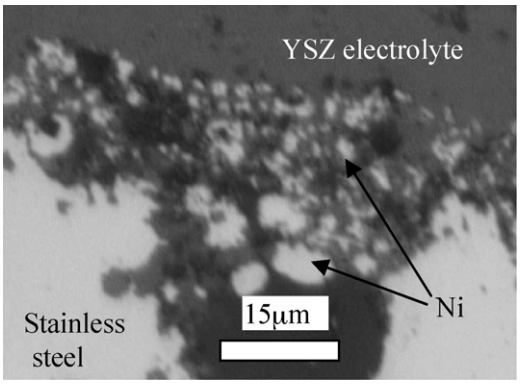

Fig. 2. Cross-section image of Ni/YSZ electrode after sintering in reducing atmosphere for 4 h at 1300 °C. Note that NiO was 3 μm maximum particle size before sintering.

Rather than accept coarsening of the Ni catalyst during cell fabrication, an alternative approach is to create a porous YSZ structure at high temperature and introduce the Ni afterwards by infiltration. Fig. 4a shows an image of very fine Ni particles infiltrated onto the walls of a porous YSZ network. Individual Ni particles are in the range 40–100 nm. A single application of the Ni precursor solution yields isolated Ni particles which are not connected to each other. This is in contrast to infiltrated LSM electrodes, which provide a well-connected LSM network in a single infiltration step [10,11]. This is simply due to the volumetric conversion rates of LSM and Ni precursor solutions. Assuming the pores of the YSZ structure are fully flooded with precursor solution during infiltration, the volume of catalyst produced after conversion from precursor to catalyst can be calculated from the concentration of transition metal in the precursor solution and density of the resulting catalyst. Whereas LSM precursor solution produces catalyst filling 15 vol% of the

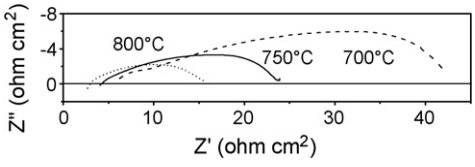

Fig. 3. AC impedance spectra of metal-support/Ni-YSZ anode/YSZ electrolyte cell cosintered at 1300 °C in reducing atmosphere for 4 h. LSCF cathode and Pt current collector was applied before cell testing with air as oxidant and moist hydrogen as fuel.

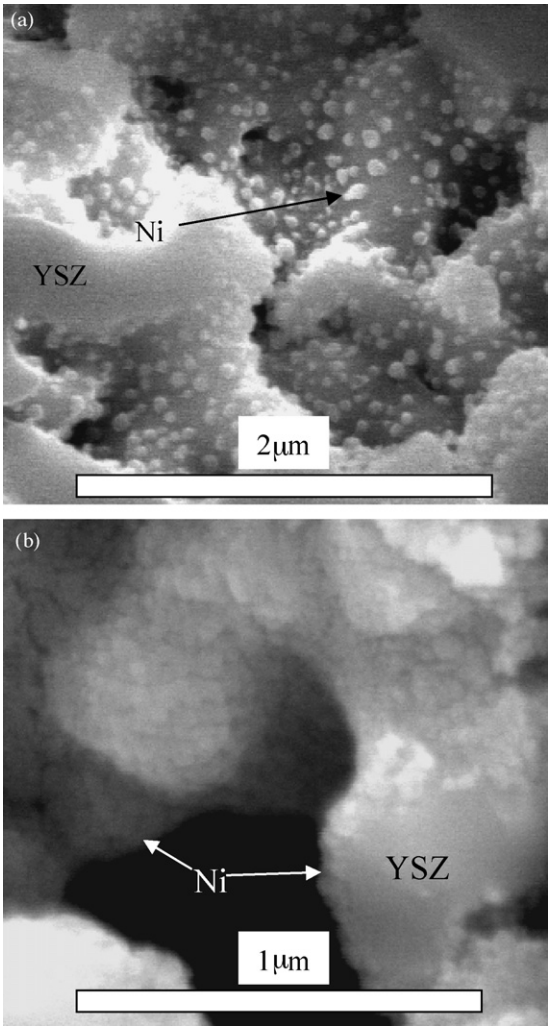

Fig. 4. SEM images of porous YSZ structures infiltrated with (a) Ni once, with Triton-X-100 surfactant, and (b) Ni five times with proprietary surfactant.

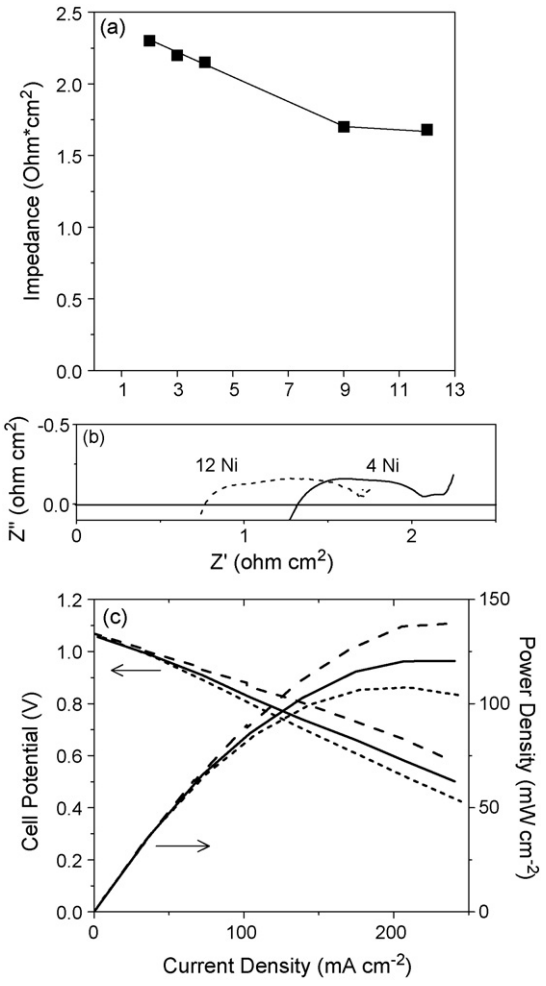

Fig. 5. Effect of number of Ni infiltration steps on performance at 700 °C with air as oxidant and moist hydrogen as fuel. (a) Total cell impedance as a function of Ni infiltration steps. (b) AC impedance spectra after 4 and 12 Ni infiltrations. (c) Polarization and power density after 1 (short dash), 4 (solid), and 12 (long dash) Ni infiltrations.

flooded pore volume after conversion from the nitrate salt to the oxide catalyst, Ni precursor solution produces catalyst filling only 3 vol% of the total pore volume. Thus, Ni precursor must be infiltrated multiple times to build up a connected network of Ni catalyst, thereby providing efficient transport of electrons throughout the anode structure. Well-connected catalyst particles can be observed after five successive infiltration steps, as shown in Fig. 4b. Note that this sample was infiltrated using Triton-X-45 surfactant in the catalyst precursor solution. This surfactant promotes the formation of smaller Ni particles, in the range 10–50 nm.

In order to assess how many Ni infiltration steps are necessary to achieve reasonable anode performance, a cell was tested after each of several successive Ni infiltration steps. The cathode was infiltrated with LSM twice and the anode was infiltrated with Ni once before testing at 700 °C. The cell was then cooled, the anode was reinfiltrated with Ni, and the cell was tested again at 700 °C. This process was repeated several times. Polarization behavior and AC impedance spectra were recorded at each testing step. The total AC impedance of the cell is shown as a function of Ni infiltration step number in Fig. 5a. The cell impedance declines rapidly with the first infiltration steps, and continues to decline moderately up to 12 infiltration steps. AC impedance, Fig. 5b, reveals that the ohmic portion of the impedance is largely responsible for the total impedance reduction upon multiple infiltrations. This is consistent with increased particle-to-particle contact with successive Ni infiltrations. For comparison, Jung et al. have reported ohmic impedance around 0.5 Ω cm^2 at 700 °C for a porous YSZ structure impregnated more than 10 times with Cu-nitrate and more than 5 times with Ce-nitrate [14]. Note that the ohmic impedance contribution of the ∼15 μm YSZ electrolyte film used here is predicted to be less than 0.1 Ω cm^2 at 700 °C and braze/manifold impedance is insignificant. Therefore, further catalyst infiltration steps beyond 12 may further decrease cell impedance. Fig. 5c shows polarization curves after 1, 4, and 12 Ni infiltration steps. Note that the open circuit potential is consistently high: the thermal cycling required to cool and reheat the cell for each infiltration step does not degrade electrolyte integrity or the quality of the braze seal. The maximum power density increases with increasing Ni content of the anode, as expected from the decreasing cell impedance.

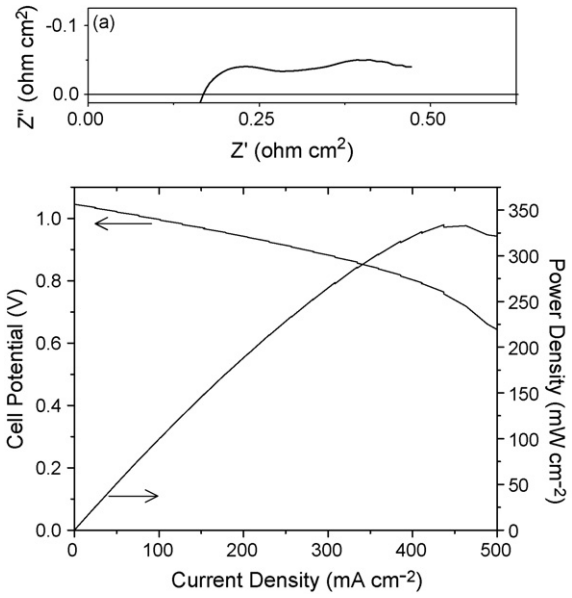

Fig. 6. Performance of cell with LSM infiltrated twice and Ni infiltrated 10 times at 700 °C with air as oxidant and moist hydrogen as fuel. (a) AC impedance spectrum and (b) polarization and power density.

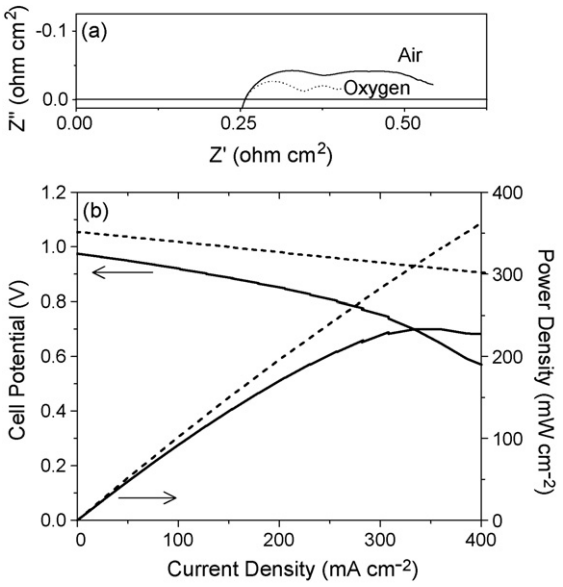

Fig. 7. Performance of cell with LSM infiltrated twice and Ni infiltrated 10 times at 650 °C with air (solid) or oxygen (dashed) as oxidant and moist hydrogen as fuel. (a) AC impedance spectra and (b) polarization and power density.

Increased performance was obtained through the use of Triton-X-45 surfactant in the infiltration precursor solution, resulting in smaller Ni catalyst particles in the porous YSZ structure, as discussed above. The following cells were all infiltrated with the improved solution. Fig. 6 shows the polarization curve for a cell with cathode infiltrated twice with LSM and anode infiltrated 10 times with Ni utilizing the improved infiltration solution. The cell achieved a maximum power density of roughly 332 mW cm^{-2} at 700 °C, with current density of 470 mA cm^{-2} produced at 0.7 V. This is the highest performance reported for a metal-supported YSZ-electrolyte cell operating at 700 °C to date. Note that the polarization is linear up to 400 mA cm^{-2}, indicating minimal activation of the catalysts in response to application of overpotential. This is desirable for easy control of an operating cell under transient load.

Fig. 7a shows cell performance for a cell infiltrated twice with LSM and 10 times with Ni, and operated at 650 °C. The cell was run with air as the oxidant, achieving 233 mW cm^{-2} at 360 mA cm^{-2}. To the best of our knowledge, this is the first reported power density for a metal-supported, YSZ-electrolyte SOFC operating below 700 °C. The oxidant stream was then switched to pure oxygen, providing a PO_2 similar to that in a pressurized SOFC operating at 5 atm. A significant increase in the performance was achieved, boosting the power density to 330 mW cm^{-2} at 360 mA cm^{-2}. A slight increase in open circuit potential (OCP) was observed when switching from air to oxygen, but certainly is not responsible for this difference in performance. AC impedance, Fig. 7b, reveals that a low-frequency process dominates the variation of cell performance with PO_2. The electrode impedance for LSM is known to vary with PO_2, decreasing 25% at 500 °C and 11% at 750 °C upon switching from air to pure oxygen [16,17]. Here, the electrode impedance decreases much more than these reported values. Furthermore, the shape of the impedance with air as oxidant suggests at least one additional process at low frequency. We therefore attribute the variation in performance with PO_2 observed here to concentration polarization and mass transport effects. Improving the structure of the cell to alleviate mass transport restriction is a subject of future work.

In order to ease the mass transport restriction, allowing the high-current performance of the infiltrated catalysts to be assessed, this cell was operated in the temperature range 650–750 °C with pure oxygen as oxidant. Fig. 8 shows the polarization behavior and AC impedance spectra at various temperatures. The maximum power achieved ranges from 982 mW cm^{-2} at 650 °C to >1300 mW cm^{-2} at 700–750 °C.

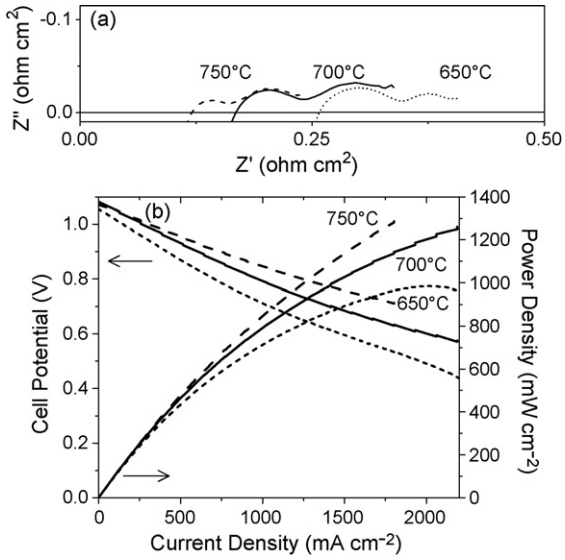

Fig. 8. Temperature-dependence of performance of cell with LSM infiltrated twice and Ni infiltrated 10 times, with oxygen as oxidant and moist hydrogen as fuel at 650 °C (short dash), 700 °C (solid), and 750 °C (long dash). (a) AC impedance spectra and (b) polarization and power density.

Power densities of 726, 993, and >1300 mW cm^{-2} were achieved at 0.7 V at 650, 700, and 750 °C, respectively. Both the ohmic and electrode impedances contribute to the thermal activation of the performance. This suggests that ionic conduction in the porous YSZ backbone of the electrodes dominates the impedance (as opposed to metallic electronic conduction in the metal-support, brazed joints, or Ni catalyst network, which would not vary significantly with temperature).

This work demonstrates that high power density can be achieved for metal-supported YSZ-based SOFCs with infiltrated electrodes. The cells tested here are roughly 1 cm diameter; we envision production-sized cells of 3 cm diameter or smaller and therefore do not expect much difficulty in scaling up the techniques used here. At the lab-scale, the most labor-intensive processing step is the multiple infiltrations required to build up a continuous network of Ni catalyst. This process occurs at relatively low temperature and does not require any specialized equipment. We therefore anticipate straightforward and inexpensive automation of this process. Future work will assess the long-term stability of this cell design.

4. Conclusions

Metal-supported SOFCs with thin YSZ electrolyte film are a robust, low-cost alternative to traditional all-ceramic SOFCs. In this work, for the first time, it is demonstrated that competitive power density can be achieved with this technology at operating temperatures that are compatible with long stainless steel lifetime. A five-layer structure consisting of porous metal-support/porous YSZ interlayer/dense YSZ electrolyte film/porous YSZ interlayer/porous metal current collector was sintered at 1300 °C in reducing atmosphere. LSM cathode and Ni anode catalysts were then infiltrated at low temperature, precluding undesirable catalyst reactions that would occur if the catalysts had been exposed to the high temperature sintering atmosphere. The resulting metal-supported SOFC with brazed seals and infiltrated catalysts supports very promising power densities. For instance, 332 and >1300 mW cm^{-2} were achieved with air and pure oxygen as oxidant, respectively, at 700 °C. Future work will focus on demonstrating longevity.

Acknowledgements

The authors gratefully acknowledge the assistance of James Wu with vacuum brazing and Teresa Chen with catalyst infiltration.

This work was supported in part by the U.S. Department of Energy under Contract No. DE-AC03-76SF00098.

References

[1] S.J. Visco, C.P. Jacobson, L.C. DeJonghe, Int. Symposium on Fuel Cells for Vehicles, Nagoya, Japan, 2000.
[2] Y. Matus, L.C. DeJonghe, C.P. Jacobson, S.J. Visco, Solid State Ionics 176 (2005) 443–449.
[3] I. Villareal, C. Jacobson, A. Leming, Y. Matus, S. Visco, L. DeJonghe, Electrochem. Solid State Lett. 6 (9) (2003) A178–A179.
[4] W.Z. Zhu, S.C. Deevi, Mater. Sci. Eng. A348 (2003) 227–243.
[5] S. Linderoth, P.H. Larsen, Mater. Res. Soc. Proc. 575 (2000) 325–330.
[6] Z.G. Yang, K.S. Weil, D.M. Paxton, J.W. Stevenson, Fuel Cell Seminar (2002) 522–525 (Abstracts).
[7] N. Christiansen, J. Hansen, H. Holm-Larsen, S. Linderoth, P. Larsen, P. Hendrikson, M. Mogensen, Fuel Cell Seminar, HI, Honolulu, 2006.
[8] J. Mizusaki, H. Tagawa, K. Baraya, T. Sasamoto, Solid State Ionics 49 (1991) 111–118.
[9] M.C. Tucker, C.P. Jacobson, L.C. DeJonghe, S.J. Visco, J. Power Sources 160 (2) (2006) 1049–1057.
[10] T.Z. Sholklapper, V. Radmilovic, C.P. Jacobson, S.J. Visco, L.C. DeJonghe, Electrochem. Solid State Lett. 10 (4) (2007) B74–B76.
[11] T.Z. Sholklapper, C. Lu, C.P. Jacobson, S.J. Visco, L.C. DeJonghe, Electrochem. Solid State Lett. 9 (8) (2006) A376–A378.
[12] T. Franco, R. Ruckdaeschel, M. Lang, G. Schiller, P. Szabo, 7th European Fuel Cell Forum, Lucerne, Switzerland, 2006.
[13] T. Franco, K. Schibinger, Z. Ilhan, G. Schiller, A. Venskutonis, ECS Transactions 7 (1) (2007) 771–780.
[14] S. Jung, C. Lu, H. He, K. Ahn, R.J. Gorte, J.M. Vohs, J. Power Sources 154 (2006) 42–50.
[15] H. Kurokawa, G.Y. Lau, C.P. Jacobson, L.C. DeJonghe, S.J. Visco, J. Mater. Proc. Tech. 182 (2007) 469–476.
[16] J.R. Smith, E.D. Wachsman, Electrochem. Acta 51 (2006) 1585–1591.
[17] E.P. Murray, et al., Solid State Ionics 110 (1998) 235–243.